

Optimal Growth Conditions for Selective Ge Islands Positioning on Pit-Patterned Si(001)

R. Bergamaschini · F. Montalenti · L. Miglio

Received: 29 June 2010/Accepted: 26 July 2010/Published online: 6 August 2010
© The Author(s) 2010. This article is published with open access at Springerlink.com

Abstract We investigate ordered nucleation of Ge islands on pit-patterned Si(001) using an original hybrid Kinetic Monte Carlo model. The method allows us to explore long time-scale evolution while using large simulation cells. We analyze the possibility to achieve selective nucleation and island homogeneity as a function of the various parameters (flux, temperature, pit period) able to influence the growth process. The presence of an optimal condition where the atomic diffusivity is sufficient to guarantee nucleation only within pits, but not so large to induce significant Ostwald ripening, is clearly demonstrated.

Keywords Stranski-Krastanow growth · Ge · Si · Patterning · Kinetic Monte Carlo

Introduction

Ge/Si(001) is often considered as the prototypical example of a system following the Stranski-Krastanow (SK) growth modality. The appearance of nanometric-sized, coherent Ge islands [1, 2] following the formation of a thin wetting layer (WL), attracted widespread attention in view of the possible role that islands could play in developing future-generation devices. Two main problems were identified soon after the first experimental evidences of islands formation were reported in the literature. On a flat Si(001) substrate, indeed, islands tend to nucleate randomly (see, e.g., the discussion in Montalenti et al. [3]), precluding the

possibility of obtaining ordered arrays. Secondly, under a wide range of deposition conditions, a bimodal distribution of islands (shallow {105} pyramids and steeper, multifaceted domes [4, 5]) is obtained. Very interestingly, better lateral ordering and size homogeneity can be achieved by growing multistacked layers of Ge islands separated by Si spacer layers (SL) [6], the key role being played by the strain field originated by buried Ge islands at the surface of the outermost SL [7]. Recently, the possibility of enhancing lateral ordering directly from the first layer of deposited islands was also explored [8]. While in all the above reported references, some degree of lateral ordering was clearly demonstrated, much better results, both in terms of islands positioning and of size distribution, have been achieved by well-tuned patterning of the Si substrate. In particular, a suitable pit-patterning produced remarkable results under appropriate deposition conditions [9]. Highly ordered, unimodal distributions of dome islands are visible in the AFM images reported in Zhong and Bauer [9]. Further evidence of nice lateral ordering can be found also in Refs. [10, 11, 12].

In this work, we further explore ordering and homogeneity of Ge islands grown on pit-patterned Si(001). More specifically, we introduce an hybrid Kinetic Monte Carlo (h-KMC) method, developed in order to expand the typical length and time scales treatable in standard KMC, and we analyze the dependence of ordering and homogeneity on key parameters such as temperature, deposition flux and pit spacing.

Model

On very general grounds, it is clear that reliable atomistic heteroepitaxial-growth simulations could strongly help in

R. Bergamaschini (✉) · F. Montalenti · L. Miglio
L-NESS and Materials Science Department,
University of Milano-Bicocca, Via R. Cozzi 53,
20125 Milano, Italy
e-mail: roberto.bergamaschini@mater.unimib.it

restricting the parameter-space to be experimentally sampled to obtain the desired result, e.g. in terms of islands distribution, positioning, etc. This is however a daunting task if one is willing to capture the whole atomic-scale complexity of Ge/Si(001) growth (with this respect, we notice that *prototypical* does not mean simple), including changes in surface reconstruction [13], long-ranged elastic fields [14], and huge spatial (experimentally determined island volumes easily reaching 10^5 nm^3 or more, pit extension and spacing being of the orders of hundreds of nm [9]) and time scales (experiments being performed at *human* time scales of several seconds). Despite the use of strong simplifications, such as solid-on-solid geometries [15] (which we shall also exploit), the gap between experiments and theory is still large. For example, standard KMC simulations [16, 17, 18] for growth on patterned substrates were reported for typical simulation-cell dimensions of 400×400 atomic sites or lower [19, 20] and were restricted to very initial stages of growth, so that a direct comparison with experiments under realistic conditions was not attempted. Nevertheless, these simulations nicely demonstrated the existence of optimal ranges of temperature and deposition flux for obtaining homogeneous and laterally ordered distributions of islands. We therefore tried to keep the essential ingredients of the above approaches, using however a faster simulation method allowing for a reduction in the gap between simulation and experiments. Although details are different, our approach is conceptually similar to the one recently proposed by Mixa et al. [21] for simulating PbSe/PbEuTe, since it also mixes atomistic and continuum descriptions.

In our model, the growth substrate is defined as a two-dimensional squared lattice, with length parameter $a \sim 4 \text{ \AA}$, corresponding to the nearest neighboring distance on (001) planes in Si. Periodic boundary conditions are applied. On this grid, we reproduce the dynamics of single atoms and islands, assuming as mobile species only isolated atoms, in order to limit the number of possible events.

Adatoms are described as in the standard KMC: they diffuse between nearest neighboring sites through thermally activated hops, as shown in Fig. 1. The hop-diffusion rate for an isolated adatom is determined by the Arrhenius relation

$$R_{\text{dif}} = v_0 \exp \left(-\frac{E_S}{kT} \right) \quad (1)$$

where v_0 is the hopping attempt frequency (here set to the standard value $v_0 = 10^{13} \text{ s}^{-1}$), E_S is the diffusion barrier, k the Boltzmann constant and T the temperature. We use $E_S = 1.1 \text{ eV}$, a value compatible with similar simulations in literature [22, 23].

Adatoms aggregates of any dimension are defined as islands, *macroscopic* entities with volume-dependent shape

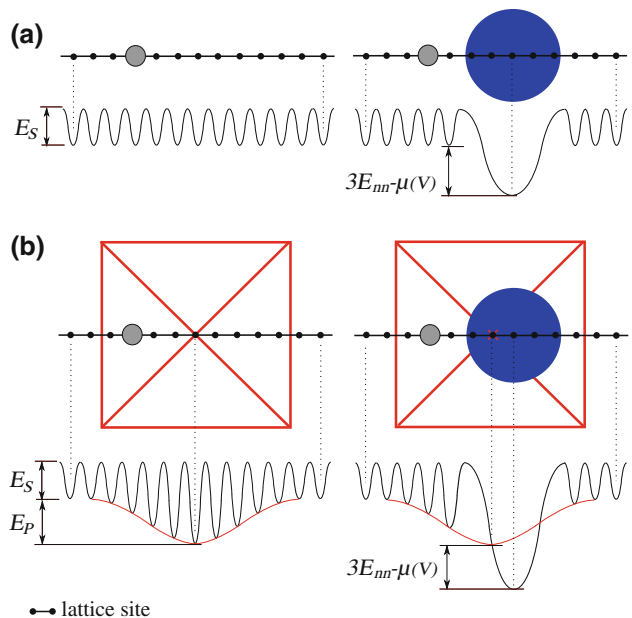


Fig. 1 Schematic representation of the potential energy profile for adatom diffusion and detachment from islands on flat regions (a) and inside pits (b)

and geometry: all the atomic motion inside an island is ignored assuming quick rearrangement processes to the mean equilibrium shape. An island nucleates once two adatoms reach the same lattice site forming a dimer and grows capturing adatoms diffused at its perimeter or directly deposited over its area. Coalescence between neighboring islands is possible too. Atomic detachment from islands is supposed to involve only atoms placed along the perimeter (as in Ross et al. [24]) through a thermally activated process whose barrier is assumed to be equal to the energy of an atom inside the island. Such quantity includes a chemical bonding contribution and an elastic and surface energy term. The former is taken equal to the interaction of an atom with the substrate E_S and with its m nearest neighbors E_{nn} . The latter should require in principle to solve the full elastic problem at each volume and configuration but, for the sake of simplicity, it is included in our model in an effective way as a chemical potential term $\mu(V)$. The effective detachment rate R_{det} for an island of volume V is then expressed as

$$R_{\text{det}} = N_p(V) v_0 \exp \left(-\frac{E_S + mE_{nn} - \mu(V)}{kT} \right) \quad (2)$$

where N_p is the number of atoms along the island perimeter. More specifically, we assume that each atom on the perimeter is bonded to three neighbors ($m = 3$, except for dimers and trimers) and for each bond we define an energy of $E_{nn} = 0.25 \text{ eV}$ (again, a common value from literature [22, 23]). Atoms removed from an island are placed in a

randomly chosen adjacent site and then treated as free adatoms. Since all events associated with islands only involve their base, the whole dynamics can be reduced to the growth plane, limiting the description to two dimensions. As a first approximation, we consider the *mean* island base as circular, with radius related to its volume. We distinguish between three typologies of structures: small 2D aggregates, {105} pyramids and domes. In the case of small atomic aggregates, for which it is not proper to consider a three-dimensional structure, we set $\mu(V) = 0$ and assimilate them to cylinders one layer high, and perimeter determined by imposing conservation of the total atomic volume (sum of the atomic volumes of the atoms composing the 2D aggregate). For size greater than 3 nm^3 , instead, we consider 3D islands. This magic value is simply determined by geometrical constraints (a {105} pyramid higher than a single (001) layer cannot occupy a smaller volume). Following the theoretical results reported in Brehm et al. [25], pyramids are transformed into domes when a critical volume of $2,400 \text{ nm}^3$ is reached, so that the transformation into a steeper morphology is energetically favored. In the simulations, pyramids and domes are treated differently both from a geometrical point of view (different base corresponding to the same volume) and for what concerns the energetics. A different island chemical potential $\mu(V)$ ($\mu_{\text{dome}} < \mu_{\text{pyr}}$ at sufficiently large V , reflecting the increased elastic-energy relaxation), also taken from Brehm et al. [25], is indeed attributed. Notice that in Ref. [25], the energy of the island as a function of the volume is reported for different WL thicknesses, the aim being to predict at what critical deposition islands start nucleating. Here however, for sake of simplicity, we shall assume a critical WL ($\sim 4 \text{ ML}$ [25]) to be already formed, using only the *thick-film limit* energy values reported in the quoted reference. Figure 1a schematically summarizes our description of the dynamics on the flat surface.

The pit pattern on the surface is included in the model defining regularly spaced square areas on the reference lattice, each corresponding to a pit, associated with an extra barrier term $E_p(x, y)$ with gaussian profile, as shown in Fig. 1b. In such a way, we obtain two effects: an increase in the nucleation probability into the pit, thanks to the slower adatoms diffusion, and a strong stabilization of islands grown there due to the reduced detachment rates. This is clearly an extremely simplified way for favoring nucleation in the pits which, as shown in Refs. [10, 26], is driven not only by capillarity effects but also by pit-induced enhanced strain relaxation. In the simulations here below described, we considered pits 20 nm wide, using gaussians with maximum amplitude of 0.2 eV and a FWHM equal to 5 nm , and pit periods ranging from 40 to 80 nm .

Results

In order to look for growth parameters ensuring positional and dimensional ordering for the islands, we have applied our h-KMC approach to a wide range of conditions.

In accordance with previous studies based on standard KMC approaches [19, 20], our simulations show the existence of an optimal range of parameters enabling both positional and size ordering in the islands grown on the patterned substrate. Figure 2 shows some snapshots taken from our simulations at different temperature, deposition flux and pit spacing. From a more quantitative point of view, the size uniformity of islands inside the pits as a function of the growth temperature can be established through the distributions shown in Fig. 3. The shown results are referred to the deposition of 1 ML of Ge. As already stressed in the previous Section, we assume that a critical ($\sim 4 \text{ ML}$ [25]) WL is already present, so that our results are representative of a true coverage of $\sim 5 \text{ ML}$.

The existence of three distinct growth regimes is rather clear from a simple visual inspection of Fig. 2. At low temperature (750 K) or high deposition flux (0.04 ML/s), there is no positional order: islands nucleate both in pits and in between, and they are non-uniform in size. Increasing the temperature or decreasing the flux, selective nucleation is achieved: mobility is now sufficient to nucleate in the energetically most favorable sites (i.e., at the center of the pits), forming stable islands and ensuring the desired positional order. If the temperature is further raised (950 K), however, communication between islands in different pits becomes important, so that some of the larger islands quickly grow at the expense of their neighbors, suppressing their growth (Ostwald ripening). As it is visible in the snapshot at high temperature in Fig. 2a, some pits remain almost empty so that the size control is poor. Consequently, the optimal regime for growth can be identified at intermediate temperature and deposition flux where it is possible to achieve good control both on island positioning and size: this condition corresponds to the case at intermediate temperature (850 K) shown in Figs. 2a and 3.

Temperature and deposition flux permit to change the evolution from a regime to the other one defining the adatom effective diffusion length: increasing temperature we exponentially enhance the hopping rate, while reducing the flux we increase the time for the adatom motion ($\propto 1/F$). Thus, while the effect of small variations in the temperature is abrupt, changing gradually the flux, as shown in panel b) of Fig. 2, we can slowly move from one regime to the other. In particular, from the figure we can notice that around each island there is a depleted region, the radius of which increases lowering the flux. Such an area roughly represents the island capture zone, and its extension with respect to the pit distance determines the growth modality.

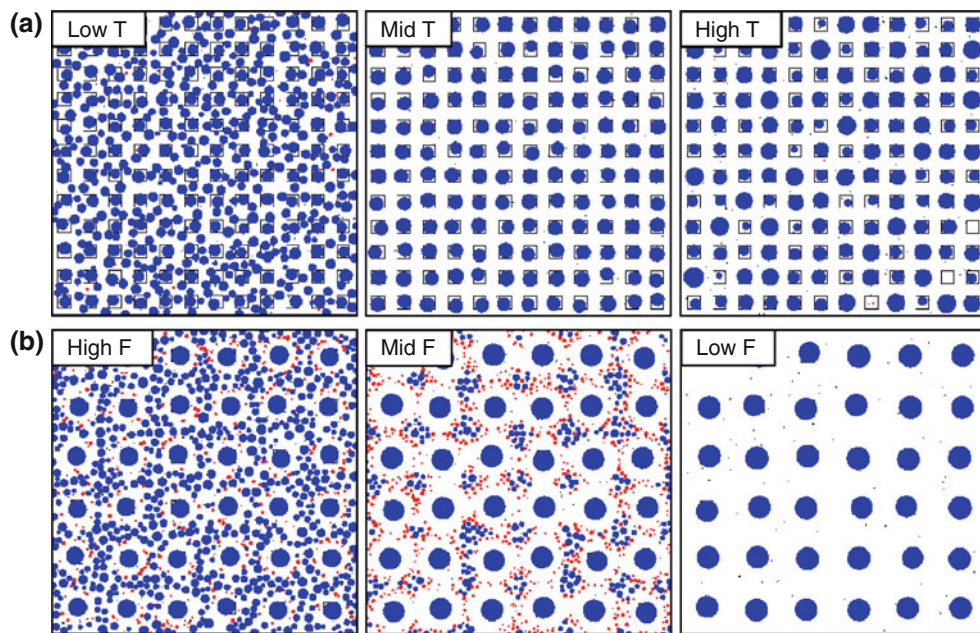


Fig. 2 Snapshots for the simulation after deposition of 1 ML of Ge on a pit-patterned substrate. Red circles represent 2D islands and blue ones are for pyramids. The surface shown corresponds to $480 \times 480 \text{ nm}^2$ (i.e., $1,200 \times 1,200$ lattice sites). **a** Growth at fixed

flux (0.02 ML/s) for pit spacing of 40 nm at three different temperatures (from left to right: $750, 850$ and 950 K). **b** Growth at fixed temperature (850 K) for pit spacing of 80 nm at three different deposition fluxes (from left to right: $0.04, 0.02$ and 0.01 ML/s)

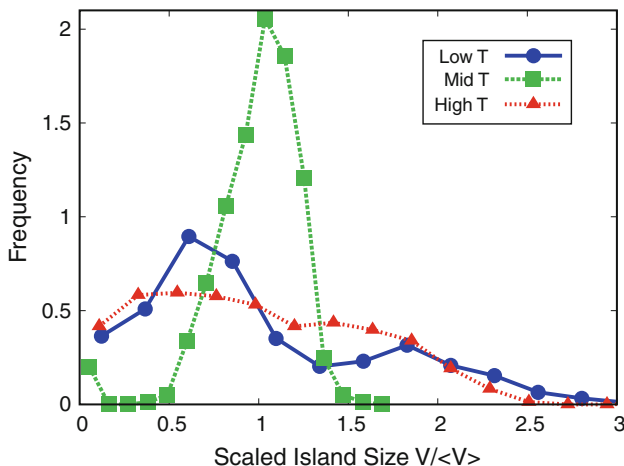


Fig. 3 Islands volume distributions from simulations at different temperatures ($750, 850$ and 950 K for the simulation parameters) at fixed flux (0.02 ML/s) and pit spacing (40 nm) after deposition of 1 ML of Ge. Curves are normalized and volumes are scaled with respect to the mean; values are averaged from 5 independent simulations. At the lowest temperature, the distribution is bimodal: the peak at larger volume is for islands inside pits, while the other refers to those grown in between.

The higher is the temperature or the lower is the flux, the wider is the region from which a pit can capture adatoms and correspondingly the smaller is the space in between where other islands can nucleate. Approximately, when capture regions of islands in adjacent pits touch all adatoms can move to pits without nucleating outside so that the

positional order is achieved. Moreover, in such a condition the region from which a pit acquires material is substantially the same for each one thus the islands grow very similar in size. Only when the growth condition gives raise to relevant overlapping in the capture areas around adjacent pits, there are competitive effects that produce ripening, as observed in the simulations at high temperature. Because the different growth regimes are determined by the ratio between the effective adatom diffusion length and pit spacing, the actual values of temperature and flux to achieve the optimal growth conditions are specific for the pattern geometry considered. This is evident comparing the two images in Fig. 2 at intermediate temperature and flux but with different pit distance.

Critical Discussion and Conclusions

Despite the enhanced realistic conditions allowed for by our model, in terms of growth temperature and deposition flux, our simulation results still suffer from some limitations which do not allow for a direct comparison with experiments, e.g. with the results of Refs. [9, 27]. The principal problem stems in the very large pit dimensions (e.g. lateral size 300 nm and depth $\sim 50 \text{ nm}$), in the large period of the patterned area ($\sim 500 \text{ nm}$ in Refs. [9, 27], see [28] for experiments performed on smaller periods), in the typical volume of the islands (10^5 nm^3) and in the presence

of phenomena occurring at large enough volumes (Si/Ge intermixing [29], onset of plasticity [30]) which are not yet included in the presented approach. Nevertheless, the present simulations offer a clear qualitative picture of the three different growth regimes [19] characterizing growth on patterned substrates. We notice that very recent, still unpublished experimental results [27] confirmed the reported transition between random nucleation, ordered nucleation and Ostwald-ripening dominated patterns.

Interestingly, at variance with the observation of Ref. [9, 27] reproduced by our model, recent experiments by Pascale et al. [12] revealed preferential nucleation sites at the pit border and not at its interior. We believe this is a strong indication of the role played by the detailed pit morphology, overlooked so far in the literature, and surely demanding for further theoretical investigations.

Open Access This article is distributed under the terms of the Creative Commons Attribution Noncommercial License which permits any noncommercial use, distribution, and reproduction in any medium, provided the original author(s) and source are credited.

References

1. Y.W. Mo, D.E. Savage, B.S. Swartzentruber, M.G. Lagally, Phys. Rev. Lett. **65**, 1020 (1990)
2. D.J. Eaglesham, M. Cerullo, Phys. Rev. Lett. **64**, 1943 (1990)
3. F. Montalenti, A. Marzegalli, G. Capellini, M. De Seta, L. Miglio, J. Phys.: Condens. Matter **19**, 225001 (2007)
4. G. Medeiros-Ribeiro, A.M. Bratkovski, T.I. Kamins, D.A.A. Ohlberg, R. Stanley Williams, Science **279**, 353 (1998)
5. F.M. Ross, R.M. Tromp, M.C. Reuter, Science **286**, 1931 (1999)
6. J. Tersoff, C. Teichert, M.G. Lagally, Phys. Rev. Lett. **76**, 1675 (1996)
7. R. Marchetti, F. Montalenti, L. Miglio, G. Capellini, M. De Seta, F. Evangelisti, Appl. Phys. Lett. **87**, 261919 (2005)
8. G. Capellini, M. De Seta, F. Evangelisti, V.A. Zinov'yev, G. Vastola, F. Montalenti, L. Miglio, Phys. Rev. Lett. **96**, 106102 (2006)
9. Z. Zhong, G. Bauer, Appl. Phys. Lett. **84**, 1922 (2004)
10. Z. Zhong, W. Schwinger, F. Schäffler, G. Bauer, G. Vastola, F. Montalenti, L. Miglio, Phys. Rev. Lett. **98**, 176102 (2007)
11. J.J. Zhang, M. Stoffel, A. Rastelli, O. G. Schmidt, V. Jovanović, L.K. Nanver, G. Bauer, Appl. Phys. Lett. **91**, 173115 (2007)
12. A. Pascale, I. Berbezier, A. Ronda, P.C. Kelires, Phys. Rev. B **77**, 075311 (2008)
13. A. Rastelli, H. von Känel, G. Albini, P. Raiteri, D.B. Migas, L. Miglio, Phys. Rev. Lett. **90**, 216104 (2003)
14. V. Holý, J. Stangl, S. Zerlauth, G. Bauer, N. Darowski, D. Lübbert, U. Pietsch, J. Phys. D: Appl. Phys. **32**, A234 (1999)
15. J.D. Weeks, G.H. Gilmer, Adv. Chem. Phys. **40**, 157 (1979)
16. A.B. Bortz, M.H. Kalos, J.L. Lebowitz, J. Comp. Phys. **17**, 10 (1975)
17. A. Voter, Phys. Rev. B **34**, 6819 (1986)
18. K.A. Fischhorn, W.H. Weinberg, J. Chem. Phys. **95**, 1090 (1991)
19. C. Lee, A.-L. Barabasi, Appl. Phys. Lett. **73**, 2651 (1998)
20. L. Nurminen, A. Kuronen, K. Kaski, Phys. Rev. B **63**, 035407 (2000)
21. M. Mixa, V. Holý, G. Springholz, G. Bauer, Phys. Rev. B **80**, 045325 (2009)
22. J. Mysliveček, C. Schelling, F. Schäffler, G. Springholz, P. Šmilauer, J. Krug, B. Voigtländer, Surf. Sci. **520**, 193 (2002)
23. T. Kawamura, T. Natori, Surf. Sci. **438**, 148 (1999)
24. F.M. Ross, J. Tersoff, R.M. Tromp, Phys. Rev. Lett. **80**, 984 (1998)
25. M. Brehm, F. Montalenti, M. Grydlik, G. Vastola, H. Lichtenberger, N. Hrauda, M.J. Beck, T. Fromherz, F. Schäffler, L. Miglio, G. Bauer, Phys. Rev. B **80**, 205321 (2009)
26. T.U. Schülli, G. Vastola, M.-I. Richard, A. Malachias, G. Renaud, F. Uhlík, F. Montalenti, G. Chen, L. Miglio, F. Schäffler, G. Bauer, Phys. Rev. Lett. **102**, 025502 (2009)
27. M. Grydlik, M. Brehm, T. Fromherz and G. Bauer, private communications
28. C. Dais, G. Mussler, H. Sigg, T. Fromherz, V. Auzelyte, H.H. Solak, D. Grützmacher, Europhys. Lett. **84**, 67017 (2008)
29. M. De Seta, G. Capellini, F. Evangelisti, J. Appl. Phys. **92**, 614 (2002)
30. A. Marzegalli, V.A. Zinov'yev, F. Montalenti, A. Rastelli, M. Stoffel, T. Merdhanova, O.G. Schmidt, L. Miglio, Phys. Rev. Lett. **99**, 235505 (2007)